19. Pritchard-Jones RO, Dunn DB, Qiu Y, et al. Expression of VEGF(xxx)b, the inhibitory isoforms of VEGF, in malignant melanoma. *Br J Cancer*. 2007;97:223-230.
20. Hua J, Spee C, Kase S, et al. Recombinant human VEGF165b inhibits experimental choroidal neovascularization. *Invest Ophthalmol Vis Sci*. 2010;51:4282-4288.
21. Magnussen AL, Rennel ES, Hua J, et al. VEGF-A165b is cytoprotective and antiangiogenic in the retina. *Invest Ophthalmol Vis Sci*. 2010;51:4273-4281.
22. Gragoudas ES, Adamis AP, Cunningham ET Jr, Feinsod M, Guyer DR. Pegaptanib for neovascular age-related macular degeneration. *N Engl J Med*. 2004;351:2805-2816.
23. Rosenfeld PJ, Brown DM, Heier JS, et al. Ranibizumab for neovascular age-related macular degeneration. *N Engl J Med*. 2006;355:1419-1431.
24. Brown DM, Kaiser PK, Michels M, et al. Ranibizumab versus verteporfin for neovascular age-related macular degeneration. *N Engl J Med*. 2006;355:1432-1444.
25. Brown DM, Michels M, Kaiser PK, Heier JS, Sy JP, Ianchulev T. Ranibizumab versus verteporfin photodynamic therapy for neovascular age-related macular degeneration: two-year results of the ANCHOR study. *Ophthalmology*. 2009;116:57-65. e55.
26. Good TJ, Kimura AE, Mandava N, Kahook MY. Sustained elevation of intraocular pressure after intravitreal injections of anti-VEGF agents. *Br J Ophthalmol*. 2010;95:1111-1114.
27. Jager RD, Aiello LP, Patel SC, Cunningham ET Jr. Risks of intravitreous injection: a comprehensive review. *Retina*. 2004; 24:676-698.
28. Amin EM, Oltean S, Hua J, et al. WT1 mutants reveal SRPK1 to be a downstream angiogenesis target by altering VEGF splicing. *Cancer Cell*. 2011;20:768-780.
29. Nowak DG, Amin EM, Rennel ES, et al. Regulation of vascular endothelial growth factor (VEGF) splicing from pro-angiogenic to anti-angiogenic isoforms: a novel therapeutic strategy for angiogenesis. *J Biol Chem*. 2010;285:5532-5540.
30. Sanford JR, Ellis JD, Cazalla D, Caceres JF. Reversible phosphorylation differentially affects nuclear and cytoplasmic functions of splicing factor 2/alternative splicing factor. *Proc Natl Acad Sci U S A*. 2005;102:15042-15047.
31. Nowak DG, Woolard J, Amin EM, et al. Expression of pro- and anti-angiogenic isoforms of VEGF is differentially regulated by known splicing and growth factors. *J Cell Sci*. 2008;121:3487-3495.
32. Koresawa M, Okabe T. High-throughput screening with quantitation of ATP consumption: a universal non-radioisotope, homogeneous assay for protein kinase. *Assay Drug Dev Technol*. 2004;2:153-160.
33. Doukas J, Mahesh S, Umeda N, et al. Topical administration of a multi-targeted kinase inhibitor suppresses choroidal neovascularization and retinal edema. *J Cell Physiol*. 2008;216:29-37.
34. Zhou Z, Gong Q, Ye B, et al. Properties of HERG channels stably expressed in HEK 293 cells studied at physiological temperature. *Biophys J*. 1998;74:230-241.
35. Cheng H, Zhang Y, Du C, Dempsey CE, Hancox JC. High potency inhibition of hERG potassium channels by the sodium-calcium exchange inhibitor KB-R7943. *Br J Pharmacol*. 2012;165:2260-2273.
36. Du CY, El Harchi A, Zhang YH, Orchard CH, Hancox JC. Pharmacological inhibition of the hERG potassium channel is modulated by extracellular but not intracellular acidosis. *J Cardiovasc Electrophysiol*. 2011;22:1163-1170.
37. Federov O, Niesen FH, Knapp S. Kinase inhibitor selectivity profiling using differential scanning fluorimetry. In: Kuster B, ed. *Kinase Inhibitors: Methods and Protocols*. New York: Humana Press; 2011:109-118.
38. Fukuhara T, Hosoya T, Shimizu S, et al. Utilization of host SR protein kinases and RNA-splicing machinery during viral replication. *Proc Natl Acad Sci U S A*. 2006;103:11329-11333.
39. Zhou Z, Qiu J, Liu W, et al. The Akt-SRPK-SR axis constitutes a major pathway in transducing EGF signaling to regulate alternative splicing in the nucleus. *Mol Cell*. 2012;47:422-433.
40. Rennel ES, Regula JT, Harper SJ, Thomas M, Klein C, Bates DO. A human neutralizing antibody specific to Ang-2 inhibits ocular angiogenesis. *Microcirculation*. 2011;18:598-607.
41. Hancox JC, McPate MJ, El Harchi A, Zhang YH. The hERG potassium channel and hERG screening for drug-induced torsades de pointes. *Pharmacol Ther*. 2008;119:118-132.
42. El Harchi A, Melgari D, Zhang YH, Zhang H, Hancox JC. Action potential clamp and pharmacology of the variant 1 Short QT Syndrome T618I hERG $K(^{+})$ channel. *PLoS One*. 2012;7: e52451.
43. McPate MJ, Duncan RS, Hancox JC, Witchel HJ. Pharmacology of the short QT syndrome N588K-hERG K^{+} channel mutation: differential impact on selected class I and class III antiarrhythmic drugs. *Br J Pharmacol*. 2008;155:957-966.
44. Aubol BE, Chakrabarti S, Ngo J, et al. Processive phosphorylation of alternative splicing factor/splicing factor 2. *Proc Natl Acad Sci U S A*. 2003;100:12601-12606.
45. Ngo JC, Chakrabarti S, Ding JH, et al. Interplay between SRPK and Clk/Sty kinases in phosphorylation of the splicing factor ASF/SF2 is regulated by a docking motif in ASF/SF2. *Mol Cell*. 2005;20:77-89.
46. Velazquez-Dones A, Hagopian JC, Ma CT, et al. Mass spectrometric and kinetic analysis of ASF/SF2 phosphorylation by SRPK1 and Clk/Sty. *J Biol Chem*. 2005;280:41761-41768.
47. Xu J, Dou T, Liu C, et al. The evolution of alternative splicing exons in vascular endothelial growth factor A. *Gene*. 2011; 487:143-150.
48. Zhao M, Shi X, Liang J, et al. Expression of pro- and anti-angiogenic isoforms of VEGF in the mouse model of oxygen-induced retinopathy. *Exp Eye Res*. 2011;93:921-926.
49. Caires KC, de Avila JM, Cupp AS, McLean DJ. VEGFA family isoforms regulate spermatogonial stem cell homeostasis in vivo. *Endocrinology*. 2012;153:887-900.
50. Harris S, Craze M, Newton J, et al. Do anti-angiogenic VEGF (VEGFxxxb) isoforms exist? A cautionary tale. *PLoS One*. 2012;7:e35231.
51. McFee RM, Rozell TG, Cupp AS. The balance of proangiogenic and antiangiogenic VEGFA isoforms regulate follicle development. *Cell Tissue Res*. 2012;349:635-647.
52. Ishida S, Usui T, Yamashiro K, et al. VEGF164-mediated inflammation is required for pathological, but not physiological, ischemia-induced retinal neovascularization. *J Exp Med*. 2003;198:483-489.
53. Geroski DH, Edelhauser HF. Drug delivery for posterior segment eye disease. *Invest Ophthalmol Vis Sci*. 2000;41: 961-964.
54. Keyt BA, Berleau LT, Nguyen HV, et al. The carboxyl-terminal domain (111-165) of vascular endothelial growth factor is critical for its mitogenic potency. *J Biol Chem*. 1996;271: 7788-7795.
55. Stalmans I, Ng YS, Rohan R, et al. Arteriolar and venular patterning in retinas of mice selectively expressing VEGF isoforms. *J Clin Invest*. 2002;109:327-336.
56. Thobe MN, Gurusamy D, Pathrose P, Waltz SE. The Ron receptor tyrosine kinase positively regulates angiogenic chemokine production in prostate cancer cells. *Oncogene*. 2010;29:214-226.
57. Das S, Anczukow O, Akerman M, Krainer AR. Oncogenic splicing factor SRSF1 is a critical transcriptional target of MYC. *Cell Rep*. 2012;1:110-117.

Research article

Inhibition of DYRK1A destabilizes EGFR and reduces EGFR-dependent glioblastoma growth

Natividad Pozo,[1] Cristina Zahonero,[1] Paloma Fernández,[2] Jose M. Liñares,[1] Angel Ayuso,[3] Masatoshi Hagiwara,[4] Angel Pérez,[5] Jose R. Ricoy,[5] Aurelio Hernández-Laín,[5] Juan M. Sepúlveda,[5] and Pilar Sánchez-Gómez[1]

[1]Neuro-oncology Unit, Instituto de Salud Carlos III-UFIEC, Madrid, Spain. [2]Instituto de Medicina Molecular Aplicada (IMMA), Universidad CEU-San Pablo, Madrid, Spain. [3]Brain Tumor Laboratory, Centro Integral Oncológico Clara Campal, Hospital de Madrid, Madrid, Spain. [4]Department of Anatomy and Developmental Biology, Graduate School of Medicine, Kyoto University, Kyoto, Japan. [5]Unidad Multidisciplinar de Neurooncología, Hospital Universitario 12 de Octubre, Madrid, Spain.

Glioblastomas (GBMs) are very aggressive tumors that are resistant to conventional chemo- and radiotherapy. New molecular therapeutic strategies are required to effectively eliminate the subpopulation of GBM tumor–initiating cells that are responsible for relapse. Since EGFR is altered in 50% of GBMs, it represents one of the most promising targets; however, EGFR kinase inhibitors have produced poor results in clinical assays, with no clear explanation for the observed resistance. We uncovered a fundamental role for the dual-specificity tyrosine phosphorylation–regulated kinase, DYRK1A, in regulating EGFR in GBMs. We found that DYRK1A was highly expressed in these tumors and that its expression was correlated with that of EGFR. Moreover, DYRK1A inhibition promoted EGFR degradation in primary GBM cell lines and neural progenitor cells, sharply reducing the self-renewal capacity of normal and tumorigenic cells. Most importantly, our data suggest that a subset of GBMs depends on high surface EGFR levels, as DYRK1A inhibition compromised their survival and produced a profound decrease in tumor burden. We propose that the recovery of EGFR stability is a key oncogenic event in a large proportion of gliomas and that pharmacological inhibition of DYRK1A could represent a promising therapeutic intervention for EGFR-dependent GBMs.

Introduction

High-grade gliomas (including glioblastomas – GBMs) are very aggressive primary brain tumors that are resistant to chemo- and radiotherapy (1). The current standard treatment for GBM includes aggressive surgical resection followed by administration of the alkylating agent, temozolomide, both concurrently and after radiotherapy. Bevacizumab, among other agents, is given as a second-line treatment after relapse (2, 3). However, this aggressive treatment is only palliative, as most deaths occur within 2 years of diagnosis, emphasizing the need to find new ways of effectively curing this cancer.

One approach is based on the cancer stem cell hypothesis. Several groups have demonstrated that there are significant differences in the differentiation status within a given GBM, with those cells resembling normal neural stem cells (NSCs) having a greater potential to initiate tumor formation and to maintain its growth (4–6). This subpopulation of cells is therefore often referred to as tumor-initiating cells (TICs). GBM-TICs share the expression of neural markers with NSCs, as well as their capacity for self-renewal and multipotent differentiation (7–9), and both of these cell types can be enriched in the same culture conditions (10). TICs have been associated with tumor relapse after therapy (11, 12) and with the invasive and proangiogenic capacity of GBM cells, two hallmarks of this type of tumor (13, 14). Therefore, therapeutic strategies that target GBM-TICs are of special interest.

The classical GBM view of mutation-driven tumors and the cancer stem cell hypothesis are reconcilable. Indeed, the key pathways in GBM (p53, PTEN, and pRB-p16) (8, 15) also play important roles in the biology of stem cells. A good example is the epidermal growth factor receptor (*EGFR*), one of the most prevalent genes altered in GBMs that is mutated and/or amplified in approximately 50% of primary tumors (16). EGF is one of the main mitogens for NSCs and, together with basic fibroblast growth factor (bFGF), it maintains the stem-like properties of both NSCs and GBM-TICs (10, 17). Indeed, it was recently shown that EGFR signaling directly controls the expression of stem cell features in GBMs (18) and that the presence of this receptor at the membrane could indicate a highly aggressive subpopulation of GBM-TICs (19). These findings reinforce the therapeutic potential of targeting EGFR in malignant gliomas.

Small-molecule tyrosine kinase (TK) inhibitors are the most clinically advanced EGFR-targeted agents to treat GBM. However, despite some initial reports on the partial efficacy of these TK inhibitors in patients with recurrent tumors (20), later studies have not been able to confirm their survival benefits (21, 22). Attempts to identify biomarkers that help predict response to EGFR inhibitors have also yielded conflicting results (22–24). It is not even clear if the levels of EGFR expression are correlated with GBM responsiveness to TK inhibitors (16), suggesting that the receptor may contribute to tumor growth independent of its kinase activity.

DYRK1A is a dual-specificity tyrosine phosphorylation–regulated kinase (DYRK) that plays an important role in the development of the central nervous system (CNS), influencing proliferation, neurogenesis, neuronal differentiation, cell death, and

Authorship note: Natividad Pozo and Cristina Zahonero contributed equally to this work.

Conflict of interest: The authors have declared that no conflict of interest exists.

Citation for this article: *J Clin Invest.* 2013;123(6):2475–2487. doi:10.1172/JCI63623.

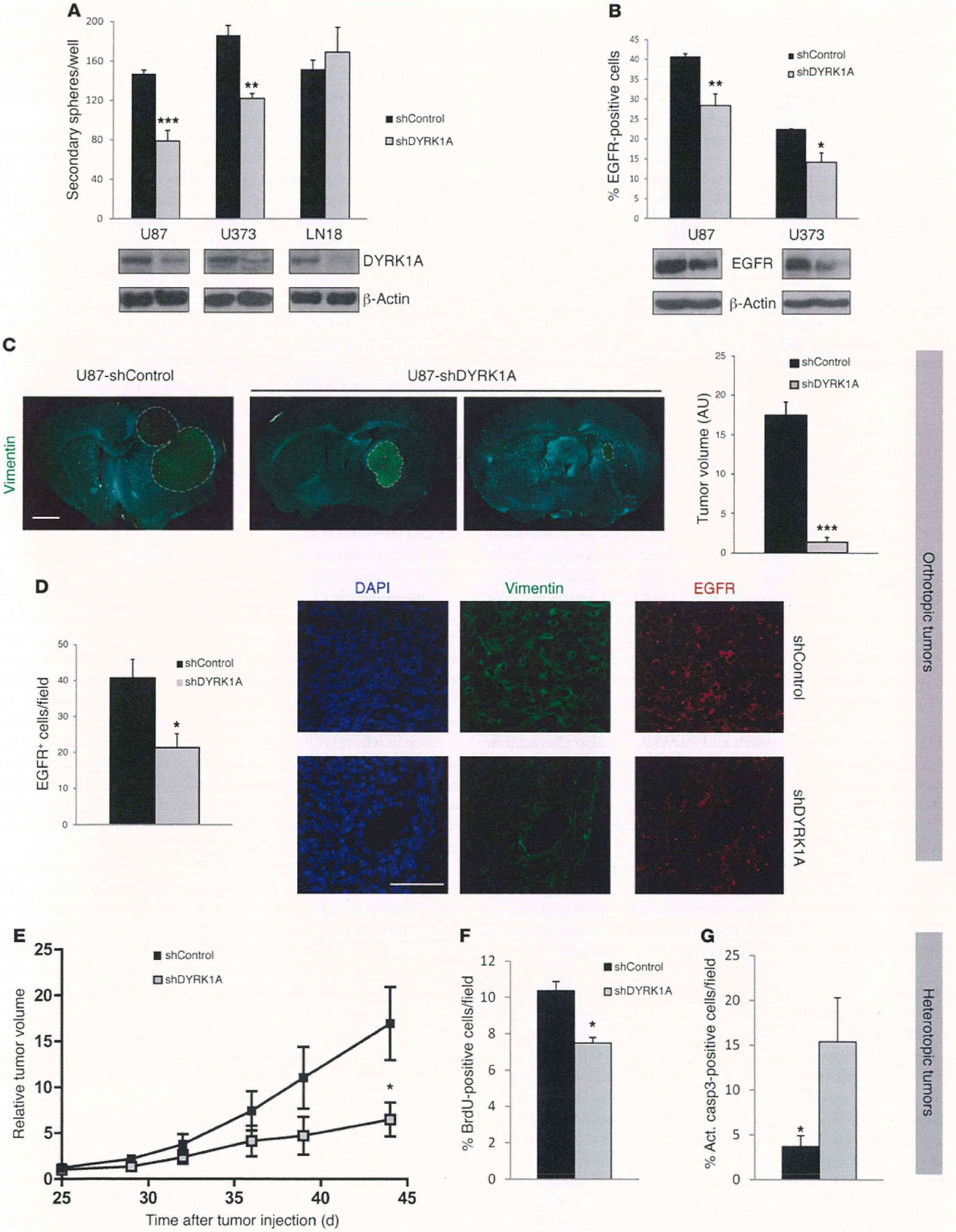

Figure 1
DYRK1A interference affects the levels of EGFR and the tumorigenic capacity of established GBM cell lines. (**A**) GBM cell lines were infected with the shControl or shDYRK1A lentivirus, and the capacity to form secondary spheres was measured. Bottom Western blot panels illustrate the inhibition of kinase expression. (**B**) Flow cytometric analysis of the percentage of EGFR-positive cells after lentiviral infection of 2 GBM cell lines. Bottom Western blot panels display the amount of total EGFR protein. (**C**) Images show representative vimentin staining of tumors formed after implantation of 10,000 puromycin-selected shControl- or shDYRK1A-infected U87 cells. Graphs on the right show the quantification of tumor volume. (**D**) Number of EGFR-positive cells per tumorigenic field, with representative images shown on the right. (**E**) Puromycin-selected shControl- or shDYRK1A-infected U87 cells (3×10^6) were implanted into the flanks of nude mice. Tumor size was measured once every 4–5 days. Relative tumor volume = tumor volume measured/tumor volume at day 25. (**F**) Proportion of BrdU-positive cells in shControl and shDYRK1A tumor tissues. (**G**) Number of activated caspase 3–positive (Act. casp3-positive) cells in the tumor tissues. Scale bars: 800 μm (**C**); 50 μm (**D**). $^*P \leq 0.05$; $^{**}P \leq 0.01$; $^{***}P \leq 0.001$.

synaptic plasticity (25, 26). DYRK1A is also expressed in the adult brain and has been linked to cognitive deficits in neurodegenerative disorders and Down syndrome (27). Interestingly, both overexpression and downregulation of DYRK1A are associated with neurological defects, reflecting the extreme gene-dosage sensitivity of this protein. Our recent data show that DYRK1A is also implicated in the maintenance and expansion of NSC pools, its haploinsufficiency eliciting defects in the self-renewal capacity of NSCs from the subventricular zone (SVZ). *Dyrk1A* heterozygous SVZ contained fewer EGFR-positive cells, leading to diminished NSC activation in response to EGF. Our data indicate that DYRK1A prevents endocytotic degradation of EGFR through the phosphorylation of the EGFR-signaling modulator Sprouty2 (SPRY2) (28).

In the present study, we found that interfering DYRK1A compromised EGFR stability in established and primary GBM cell lines, affecting tumor growth and survival. We also characterize the important expression of DYRK1A in astrocytic tumors, especially in those that contain high levels of EGFR, and we confirm that DYRK1A inhibition promotes EGFR degradation. Moreover, DYRK1A determined the duration of receptor signaling, its inhibition strongly and irreversibly inhibiting self-renewal in receptor-dependent GBMs. Finally, we demonstrate that pharmacologically blocking DYRK1A kinase activity clearly impairs tumor growth in sensitive lines. We believe that our results allow us to propose, for the first time, that DYRK1A is a promising therapeutic target in GBMs, at least for those depending on EGFR signaling.

Results

DYRK1A modulates EGFR protein levels and the self-renewal of established GBM cell lines. To understand the role of DYRK1A in GBMs, we first silenced this kinase in established cell lines, grown in the form of neurospheres. The loss of DYRK1A inhibited the self-renewal capacity of U87 and U373 cells, although it did not affect LN18 cells (Figure 1A). Moreover, DYRK1A inhibition strongly reduced the levels of EGFR, evident in Western blots of U87 and U373 cell extracts and as assessed by cytometry of puromycin-selected cells (Figure 1B). This reduction was produced by posttranslational modifications, as lentiviral shDYRK1A did not affect the expression of the *EGFR* gene (Supplemental Figure 1A; supplemental material available online with this article; doi:10.1172/JCI63623DS1). The absence of an effect in LN18 cells could reflect the low levels of EGFR surface expression by this cell line (3.4 ± 0.2 % of positive cells) when compared with the sensitive cell lines. Furthermore, reducing DYRK1A did not influence BrdU incorporation in U87 cells (Supplemental Figure 1B), suggesting that it specifically modulates the self-renewal capacity of GBM cells as in normal NSCs (28).

DYRK1A influences U87 tumor growth. We next assessed whether the effect of DYRK1A inhibition in vitro was reflected in the capacity of GBM neurospheres to form tumors. After checking DYRK1A downregulation, we orthotopically transplanted 10,000 puromycin-selected U87 cells infected with shControl or shDYRK1A lentivirus into nude mice. There were phenotypic signs of disease 6 weeks after intracranial injection, when the animals were sacrificed and the tumor cells detected with a human-specific vimentin antibody. The tumors generated by shDYRK1A cells were much smaller (80% reduction) than those generated by shControl cells (Figure 1C), and immunostaining revealed that shDYRK1A neoplastic tissue contained fewer EGFR-positive cells (Figure 1D), suggesting that DYRK1A downregulation affected EGFR stability in vivo. We performed a competition assay by transplanting a small number of GFP-labeled shControl cells (1,000 cells) along with shDYRK1A cells (9,000 cells), at a ratio of 1:9, into the brains of nude mice. The tumors that arose 1 month later contained approximately 60% of GFP-labeled cells (Supplemental Figure 2), supporting the notion of a lower tumorigenic capacity of cells with reduced levels of DYRK1A.

To further confirm that DYRK1A levels modulate tumor growth, 3×10^6 U87 cells (shControl or shDYRK1A infected) were implanted subcutaneously into the flanks of nude mice. Notably, shDYRK1A cells did not form tumors in 2 of 6 animals, whereas shControl cells had a 100% penetrance rate in terms of tumor formation. Moreover, shDYRK1A tumors grew more slowly than their shControl counterparts, provoking a significant difference at the final endpoint ($n = 6$ [shControl], $n = 4$ [shDYRK1A]; $P = 0.0381$) (Figure 1E). Our analysis of the tumor tissue revealed that there was less proliferation in tissue in which DYRK1A interfered (Figure 1F) and significantly higher numbers of apoptotic cells (Figure 1G). Together, these data indicate that reducing the amount of DYRK1A affects EGFR levels and impairs the self-renewal capacity of GBM cells in vitro. Moreover, the results suggest that high levels of DYRK1A are necessary to maintain tumor growth and survival in vivo.

DYRK1A is strongly expressed in a subset of gliomas and its expression is correlated with EGFR levels. Although several groups have reported that DYRK1A is expressed in the adult mammalian brain in both neurons and astrocytes (29, 30), this kinase has not been identified in astrocytic tumors. Given the strong effect of DYRK1A downregulation on glioma cell lines, we set out to explore the transcript levels of *DYRK1A* in normal tissue (obtained from surgery on epileptic patients) and in a panel of gliomas of different grades by quantitative RT-PCR (qRT-PCR). The results showed a higher expression of *DYRK1A* in gliomas (especially oligodendrogliomas [ODGs] and GBMs), although with a certain degree of variability among the tumors tested (Figure 2A).

We investigated the expression of *EGFR* in the same tissue samples and, unsurprisingly, *EGFR* levels were very high in GBMs when compared with normal tissue, probably due to the high frequency of genomic amplification in such tumors (16). The *EGFR* gene was also strongly expressed in low-grade astrocytomas and even more so in ODGs, suggesting that increased EGFR expression was common in gliomas of different grades and that it was

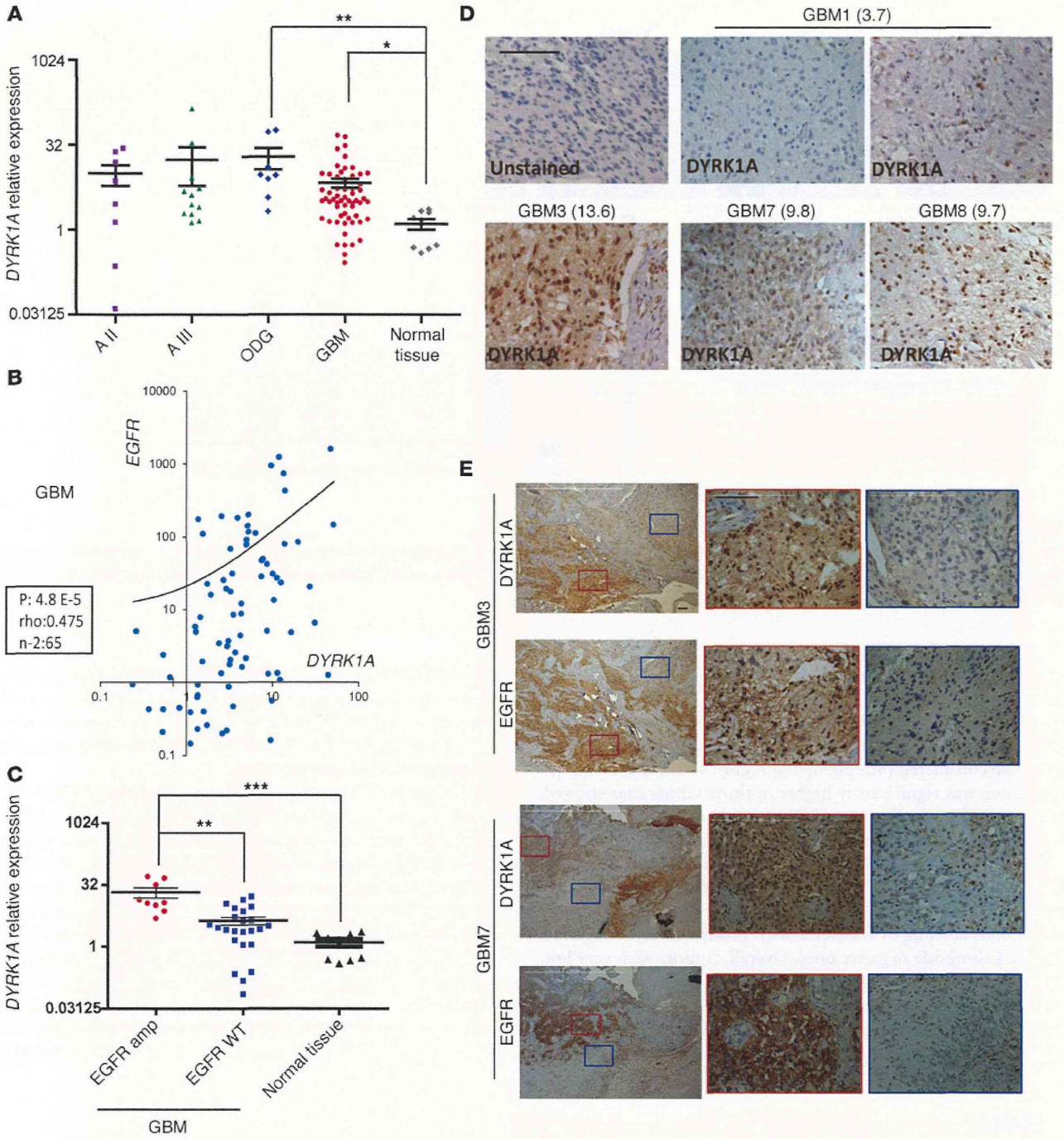

Figure 2

DYRK1A is highly expressed in a subset of gliomas and correlates with EGFR expression. (**A**) *DYRK1A* transcript levels were determined by RT-PCR in glioma samples and normal tissue (obtained during surgery on epileptic patients). *HPRT* expression was used for normalization. (**B**) Correlation between the levels of *EGFR* and *DYRK1A* transcription in the GBM samples. Spearman's rank correlation parameters are presented in the box. (**C**) Relative *DYRK1A* expression in *EGFR*-amplified (amp) and wild-type (WT) GBM samples. (**D**) IHC images showing an unstained control and 5 representative images of DYRK1A staining of 4 different GBMs. Relative DYRK1A RT-PCR values are shown in the brackets. (**E**) Low-magnification images of DYRK1A and EGFR staining of 2 different GBMs. Areas of positive (red box) and negative (blue box) staining of both markers are shown at higher magnification. A, astrocytomas. Scale bars: 50 μm. $^{*}P \leq 0.05$; $^{**}P \leq 0.01$; $^{***}P \leq 0.001$.

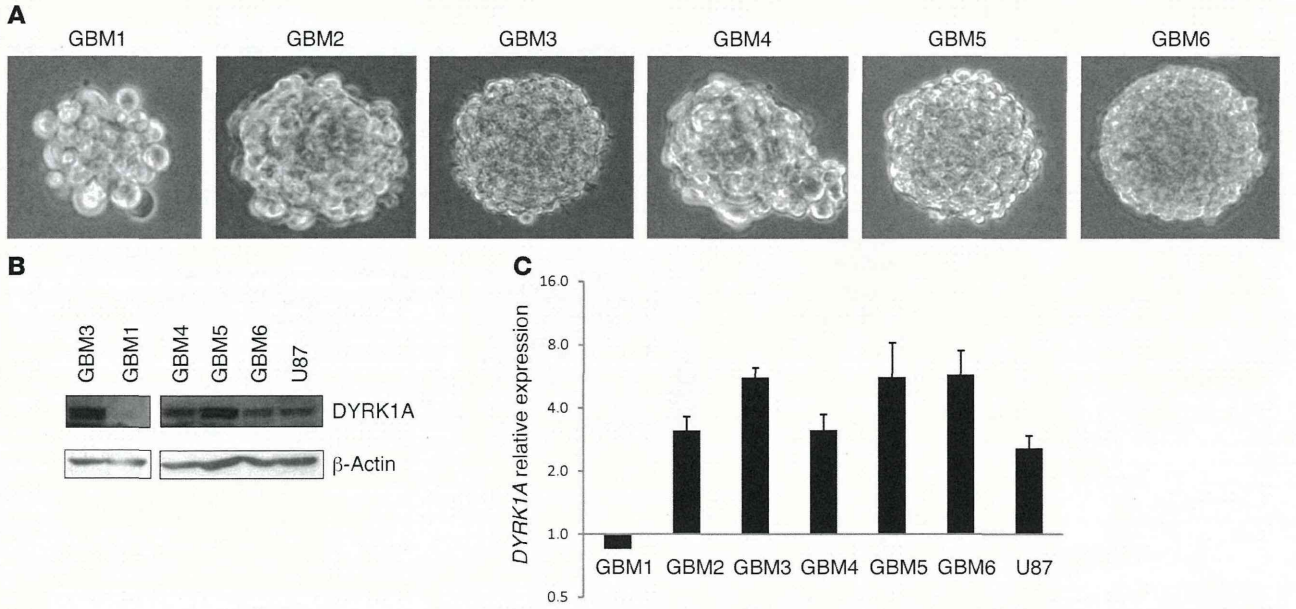

Figure 3
Characterization of the GBM-TICs used in this study. (**A**) Representative phase-contrast images of the different GBM-TICs. (**B**) DYRK1A protein expression in some of the GBM-TIC lines and U87 cells. (**C**) *DYRK1A* transcriptional levels relative to *HPRT*. Expression of *DYRK1A* in normal tissue was used for normalization.

not only caused by gene amplification (Supplemental Figure 3), as proposed elsewhere (31). Intriguingly, there was a remarkable positive correlation between *DYRK1A* and *EGFR* mRNA levels in GBMs (Figure 2B), which was even stronger when gliomas of lower grades were also considered (Supplemental Figure 4). Indeed, DYRK1A expression was significantly higher in those GBMs that showed EGFR amplification (Figure 2C). These analyses suggest that there are 2 subgroups of GBMs with regard to DYRK1A presence.

To obtain more evidence of the relationship between DYRK1A and EGFR, we analyzed paraffin-embedded tumors by immunohistochemistry (IHC). GBM tumor cells exhibited heterogeneous labeling of DYRK1A, with positive areas of staining detected alongside negative ones. Overall, tumors with very low *DYRK1A* mRNA expression (GBM1) were almost entirely negative for DYRK1A staining, whereas *DYRK1A*-expressing tumors displayed many areas of positive IHC labeling (Figure 2D). Additionally, IHC analysis confirmed that most of the samples with positive DYRK1A staining also exhibited strong EGFR expression and that even within a given tumor, DYRK1A was found mostly in areas of strong EGFR staining (Figure 2E). Altogether, these data suggest that DYRK1A function is especially relevant for the EGFR-dependent subtype of GBMs.

DYRK1A interference suppresses the self-renewal capacity of GBM-TICs. Considering the results of DYRK1A interference in GBM cell lines and the expression of this kinase in human tissue, we evaluated whether DYRK1A levels modulated the behavior of the TICs, enriched in neurosphere culture conditions, that are responsible for tumor growth and relapse (Figure 3A). All the primary lines used in this study could form tumors with high penetrance when injected into nude mice. The levels of membrane EGFR were measured by flow cytometry (Supplemental Figure 5), and 2 distinct subgroups of GBM lines were identified, as recently demonstrated, based on the different levels of EGFR surface expression (19). One of the lines used in this study had very low levels of EGFR (GBM1),

Table 1
Genetic background and surface EGFR expression of the different primary GBM-TICs used in this study

Cell line	Patient code	Origin	*EGFR* amp (genomic qPCR)	% EGFR-positive (cytometry)	PTEN loss (WB)	P53 mutation (WB and IHC)
GBM1	120-02	12 de Octubre	0	3.8 ± 2.3	1	1
GBM2	120-15	12 de Octubre	0	14.5 ± 1.9	0	1
GBM3	120-01	12 de Octubre	1	27.9 ± 4.0	0	0
GBM4	L0627	Mazzoleni et al.	1	41.7 ± 2.2	0	1
GBM5	L0605	Mazzoleni et al.	1	55.2 ± 1.2	1	0
GBM6	L0306	Mazzoleni et al.	1	64.8 ± 2.6	0	0

Primary cultures were obtained by dissociation of human GBM specimens from Hospital 12 de Octubre (12 de Octubre) or were donated by Rosella Galli (Mazzoleni et al., ref. 19). 0/1 indicates the absence or presence of the mutation. WB, Western blot.

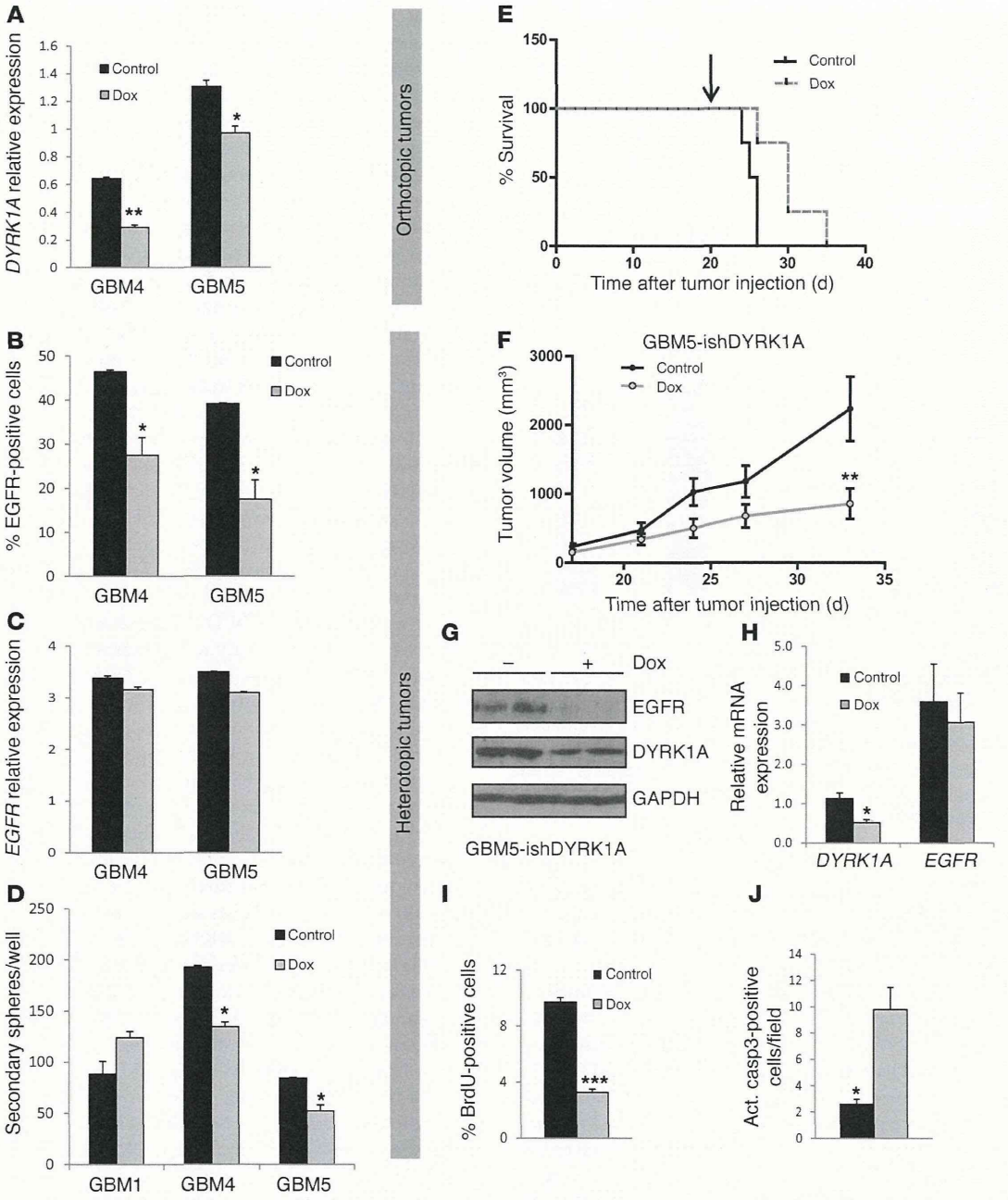

Figure 4

Conditional DYRK1A interference affects EGFR levels and the tumorigenic capacity of GBM-TICs. (**A**) RT-PCR analysis of *DYRK1A* transcripts 3 days after shDYRK1A induction with doxycycline (Dox). (**B**) Flow cytometric analysis of the amount of EGFR-positive cells 3 days after shDYRK1A induction. (**C**) RT-PCR analysis of *EGFR* transcripts 3 days after shDYRK1A induction. (**D**) Quantification of the capacity to form secondary spheres after doxycycline removal. (**E**) 50,000 GBM5 cells infected with inducible shDYRK1A (GBM5-ishDYRK1A) cells were implanted intracranially into nude mice, and 3 weeks later, doxycycline (indicated with an arrow) was added to the drinking water of 1 group of mice. Animal survival was evaluated using a Kaplan-Meier survival curve, and the differences in survival times were analyzed with a log-rank test ($n = 4$; $P = 0.0316$). (**F**) GBM5-ishDYRK1A cells (3.5×10^6) were injected into the flanks of nude mice. Two weeks later, doxycycline was added to the drinking water of 1 group of mice, and tumor size was measured once every 4–5 days. Graph represents the tumor volume after doxycycline addition. (**G**) Western blot analysis of DYRK1A and EGFR protein levels in control and doxycycline-treated tumors. (**H**) RT-PCR analysis of *DYRK1A* and *EGFR* transcript levels in control and doxycycline-treated tumors. (**I**) Number of BrdU-positive cells in the flank tumors. (**J**) Amount of cells with activated caspase 3 in the flank tumors. $^*P \leq 0.05$; $^{**}P \leq 0.01$; $^{***}P \leq 0.001$.

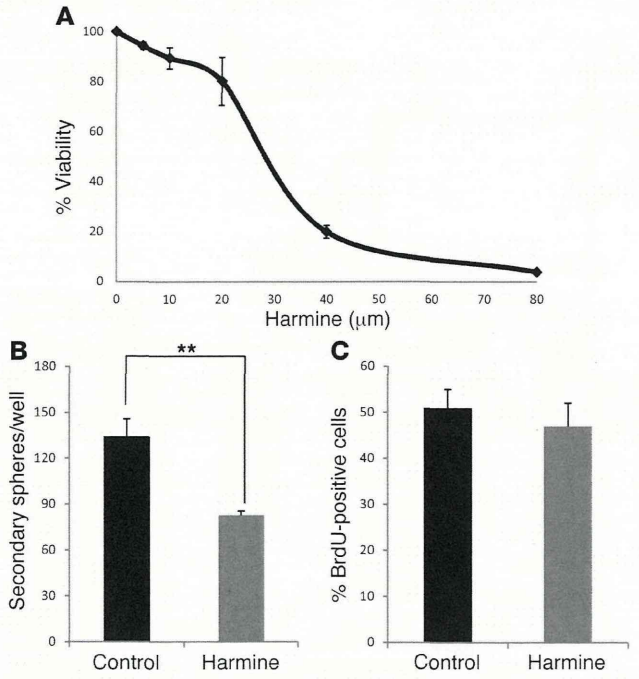

Figure 5

Harmine impairs the self-renewal capacity of SVZ-NSCs. (**A**) SVZ neurospheres were treated for 2 days in the presence of different concentrations of harmine, and cell viability was measured with a colorimetric WST-1 assay. Percentage of inhibition is represented in the graph. (**B**) Formation of secondary spheres after pretreatment with harmine (20 μm for 2 days). $^{**}P \leq 0.01$. (**C**) Percentage of BrdU-positive cells in control and harmine-treated cells.

whereas the rest had a higher proportion of EGFR-expressing cells, ranging from 15% to 65% (Table 1). DYRK1A expression was observed in all but 1 line (GBM1), as measured by Western blot analysis (Figure 3B) and RT-PCR (Figure 3C).

To test DYRK1A function in GBM-TIC–enriched cell lines, we again used an RNA interference strategy. However, we were not able to downregulate DYRK1A in the primary cultures using lentiviral constructs and selection of stably-expressing shDYRK1A cells, so we decided to use a conditional approach. The expression of the red fluorescence protein (RFP) reporter was used to track infected cells. Incubation with doxycycline induced a partial reduction in *DYRK1A* mRNA levels (Figure 4A), which was correlated with a strong reduction in the amount of EGFR-expressing cells (Figure 4B) without altering the expression of *EGFR* transcripts (Figure 4C). Three days after shDYRK1A induction, the spheres were dissociated and plated again at a clonal dilution in the absence of doxycycline. DYRK1A interference clearly inhibited the self-renewal capacity of GBM4 and GBM5 cells, but not GBM1 cells, which did not express DYRK1A and have the lowest levels of EGFR (Figure 4D). These data suggest that DYRK1A levels are essential for the expansion of EGFR-expressing GBMs, as downregulation of DYRK1A irreversibly affected the clonal growth of TICs.

DYRK1A interference suppresses the tumorigenic capacity of GBM-TICs. To address whether the effect of DYRK1A inhibition observed in vitro translated into a decreased capacity of primary GBM cells to form tumors, 50,000 puromycin-selected shDYRK1A-infected GBM5 cells were transplanted into the brains of nude mice. Three weeks later, the mice were divided into 2 groups, with doxycycline being administered to one of the groups. Kaplan-Meier analysis demonstrated that DYRK1A downregulation prolonged the survival of the GBM-bearing animals. (Figure 4E). To further analyze the effect of DYRK1A interference on the growth of GBM-TICs in vivo, we injected 3.5×10^6 infected cells into the flanks of nude mice, and when tumors reached a minimal volume, the animals were separated into 2 groups: control and doxycycline-treated mice, and were followed for 3 additional weeks before tumor analysis. Since tumors from the doxycycline-treated animals were much smaller at the final endpoint, this approach demonstrated that the induction of shDYRK1A clearly inhibited tumor progression (Figure 4F and Supplemental Figure 6). Subsequent analysis of the tumor tissue confirmed the downregulation of DYRK1A protein after doxycycline treatment, which correlated with a significant reduction in EGFR protein (Figure 4G) but not of *EGFR* mRNA transcripts (Figure 4H). As in U87 cells, BrdU was incorporated at a much lower level into shDYRK1A tumors (Figure 4I), and we observed a clear induction of apoptosis (Figure 4J). These results indicate that DYRK1A controls GBM-TIC expansion in vivo and that silencing this kinase prevents GBM growth and survival, thereby decreasing the tumor burden.

Pharmacological inhibition of DYRK1A kinase activity blocks the self-renewal capacity of GBM-TICs and impairs tumor burden. To explore the therapeutic potential of DYRK1A, it was important to clarify whether its kinase activity was necessary for the self-renewal of normal and tumorigenic stem cells. Therefore, we assessed the influence of DYRK1A inhibitor, the β-carboline alkaloid known as harmine (32) (shown to work in vivo; ref. 33). We first tested the effects of harmine on the growth properties of SVZ-NSCs. Interestingly, harmine (20 μm) had only a small effect on gross viability (Figure 5A), but it significantly inhibited the formation of secondary spheres (grown in the absence of the drug; Figure 5B) without affecting BrdU incorporation (Figure 5C). These results confirm our previous findings and further prove that pharmacological inhibition of DYRK1A inhibits stem cell behavior (28).

To determine whether DYRK1A inhibition affected the behavior of gliomas, GBM-TIC lines were maintained in the presence of harmine for 3 days, before isolating single cells from dissociated spheres and replating them at clonal densities in the absence of the drug. Harmine significantly inhibited self-renewal in most of the primary lines (Figure 6A). As shown in Figure 6B, similar effects were obtained with another DYRK1A inhibitor, INDY, a benzothiazole compound (34). Notably, neither harmine nor INDY greatly suppressed self-renewal in the DYRK1A-negative GBM1.

To further prove the oncogenic capacity of DYRK1A and determine the potential therapeutic benefit of targeting its activity in GBM-TICs, we injected 50,000 GBM5 cells into the brains of nude mice. Two weeks later, the animals were treated systemically with harmine (15 mg/kg/day, 5 days per week) or vehicle alone (saline), and their survival rates were monitored. A Kaplan-Meier analysis suggested that there is a protective effect of harmine, though it did not reach significance (Figure 6C). Unfortunately, we could not test higher doses of the drug, as they caused tremors in the animals due to the drug's ability to target monoamine oxidase (35). Nevertheless, after harmine treatment, brain tumors showed a clear reduction in cell proliferation (Figure 6D), as well as the appearance of numerous apoptotic areas (Figure 6E). Interestingly, harmine-treated tissue also showed a clear decrease in EGFR staining (Figure 6F). Therefore, DYRK1A kinase activity regulated the survival of TICs and the oncogenic capacity of EGFR-dependent GBMs.

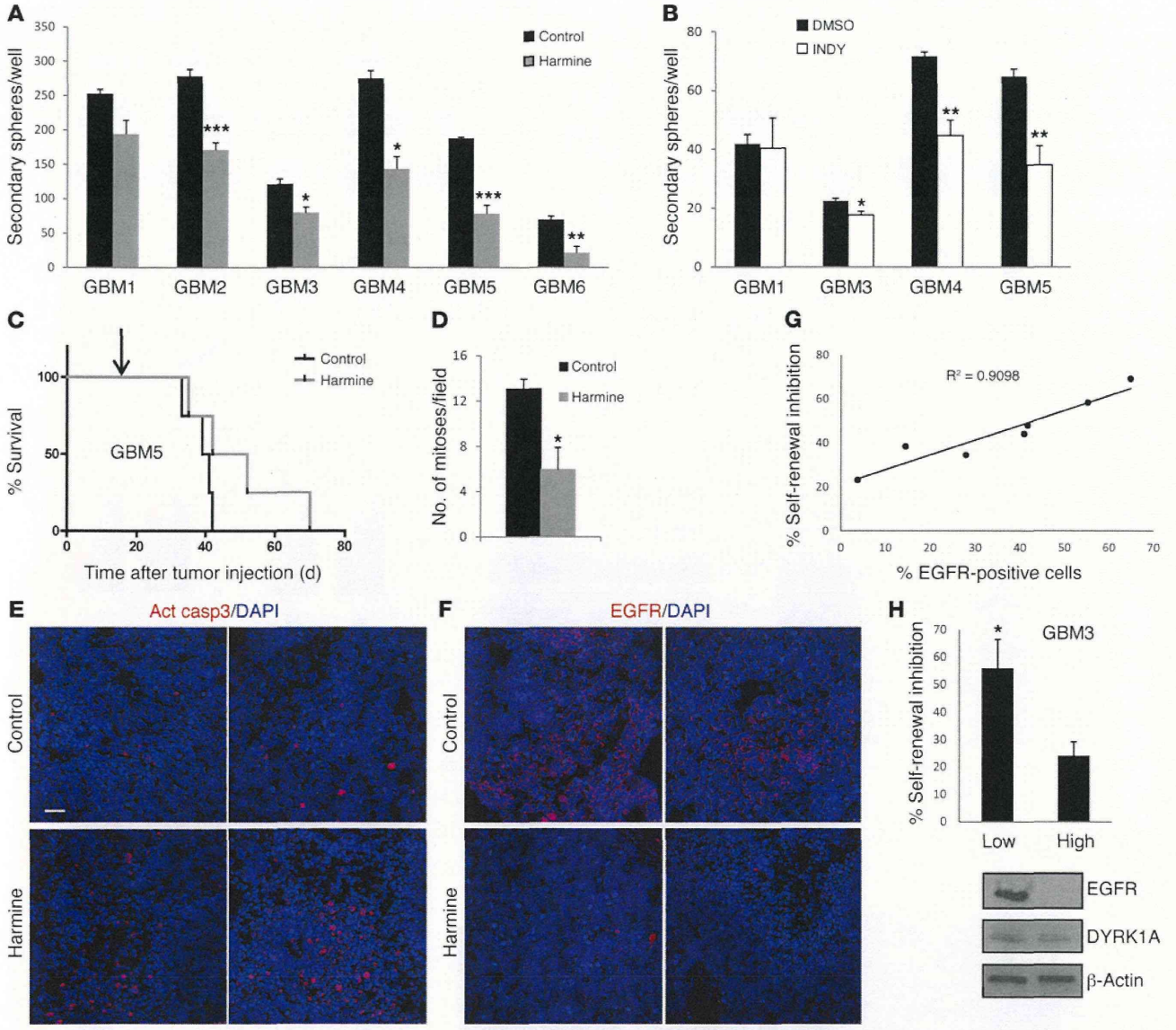

Figure 6

Pharmacological inhibition of DYRK1A impairs the self-renewal capacity of EGFR-expressing GBM-TICs. GBM primary cells were incubated in the presence of (**A**) harmine or (**B**) INDY, and 3 days later, the spheres were dissociated and replated in the absence of the drug. A 20-μm concentration was chosen based on SVZ-NSC behavior (Figure 5A and Supplemental Figure 7). The number of secondary spheres is represented in the graphs. (**C**) 50,000 GBM5 cells were implanted intracranially into nude mice. Two weeks later, the animals started to receive i.p. injections of saline (Control) or harmine (15 mg/kg/day, 5 days per week; indicated by an arrow). Animal survival was evaluated using a Kaplan-Meier survival curve, and the differences in survival times were analyzed with a log-rank test ($n = 5$; $P = 0.09$). (**D**) Number of mitotic cells in control or harmine-treated tumor tissue. (**E**) Representative images of activated caspase 3 staining in control and harmine-treated tumor tissue. (**F**) Representative images of EGFR staining in control and harmine-treated tumor tissue. (**G**) Correlation between the amount of membrane EGFR present in the different GBM-TIC lines and the percentage of self-renewal inhibition induced by harmine. (**H**) Percentage of self-renewal inhibition induced by harmine in low- or high-passage GBM3 cells. Western blot on the right shows the amount of EGFR and DYRK1A expressed by low- and high-passage GBM3 cells. Scale bar: 40 μm. $^*P \leq 0.05$; $^{**}P \leq 0.01$; $^{***}P \leq 0.001$.

The effect of harmine on GBM-TIC self-renewal depends on EGFR expression. We investigated the genetic background of our panel of GBM-TIC lines in an attempt to identify any specific pattern that could predict the response to DYRK1A inhibition, other than the presence of the protein itself in the tumor cells. We found that harmine could inhibit secondary clonal formation, regardless of PTEN deficiency or p53 mutations (Table 1), two classic GBM alterations. However, there was a very significant positive correlation between surface EGFR expression and harmine sensitivity (Figure 6G). This strongly reinforces the hypothesis that DYRK1A function modulates self-renewal of EGFR-dependent GBMs, as suggested by our earlier studies. To further confirm this proposal, we used one of the

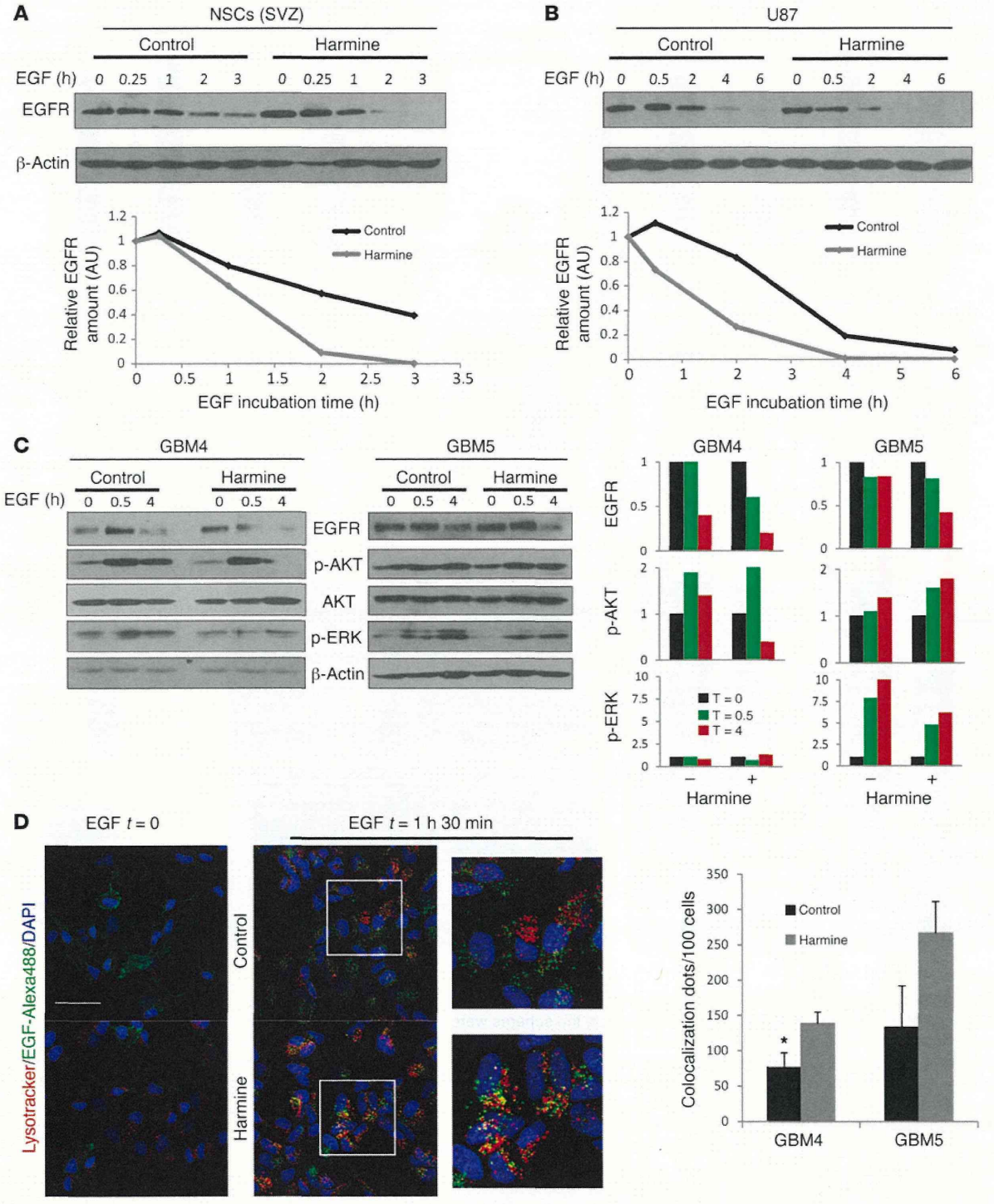

Figure 7

DYRK1A inhibition stimulates EGFR lysosomal degradation and termination of EGF signaling. Western blot analysis of SVZ-NSCs (**A**) or U87 cells (**B**) that were deprived of growth factors for 12 hours and then exposed to EGF for the indicated durations in the presence or absence of harmine. Quantification of EGFR levels relative to β-actin is shown in the bottom graphs. (**C**) Western blot analysis of the EGFR signaling pathway after EGF stimulation of 2 different GBM-TIC lines in the presence or absence of harmine. Quantification of EGFR, p-AKT, and p-ERK1/2 levels relative to β-actin is shown on the right. (**D**) GBM-TICs were preincubated in the presence or absence of harmine. Four hours later, EGF Alexa488 was added and the cells were fixed at $t = 0$ or $t = 1$ hour, 30 minutes. Representative confocal images of EGFR lysosomal targeting in GBM4 cells are shown. Quantification of the yellow dots for 2 different GBM-TIC lines is represented by the graph on the right. *$P \leq 0.05$. Scale bar: 25 μm.